JOURNAL OF AIRCRAFT
Vol. 44, No. 1, January–February 2007

Transient and Limit Cycle Simulation of a Nonlinear Aeroelastic System

C. C. Marsden* and S. J. Price†
McGill University, Montréal, Québec H3A 2K6, Canada

DOI: 10.2514/1.21367

The transient and steady-state response of an experimental aeroelastic system to initial displacements in each of its two degrees of freedom is modeled mathematically. The experimental results are from subsonic wind-tunnel tests performed on a 2-degree-of-freedom wing section with a structural, freeplay-type nonlinearity in the pitching degree of freedom. The system is modeled mathematically, and the equations of motion for the linear and three different nonlinear configurations are solved numerically to produce time histories of the wing section displacements in pitch and plunge. Numerical data are compared to experimental results for both the transient and the steady-state stable and unstable limit-cycle oscillations of the experimental apparatus. The mathematical model is modified to reflect the mass distribution and frictional forces present in the experimental apparatus, and the model is validated for the system transient response by comparing numerical and experimental time histories.

Nomenclature

a_h	=	nondimensional distance measured from the airfoil midchord to the elastic axis
b	=	airfoil semichord
c_h	=	translational viscous damping coefficient in plunge
c_α	=	torsional viscous damping coefficient in pitch
F_h	=	frictional force in plunge
F_p	=	frictional forces in pitch
h	=	plunge displacement of the airfoil section
I_α	=	moment of inertia of the airfoil section about the elastic axis
K_h	=	linear structural stiffness in plunge
K_α	=	linear structural stiffness in pitch
m_h	=	moving mass in plunge
m_p	=	moving mass in pitch
m_0	=	restoring moment preload for freeplay structural stiffness
m_1	=	airfoil section linear traveler system mass per unit span
m_2	=	airfoil section and pitching mechanism mass per unit span centered on the elastic axis
m_3	=	airfoil section only mass located at a distance bx_α from the elastic axis
r_α	=	nondimensional radius of gyration of the airfoil section about the elastic axis
U	=	nondimensional freestream velocity, $V/b\omega_\alpha$
V	=	freestream velocity
x_α	=	nondimensional distance from the airfoil center of mass to the elastic axis
α	=	pitch rotation of the airfoil section, measured about the elastic axis
α_f	=	α at the start of the freeplay region
δ	=	length of the freeplay region in the structural restoring moment
ζ_α	=	viscous damping ratio in pitch, $c_\alpha/2I_\alpha\omega_\alpha$
ζ_ξ	=	viscous damping ratio in plunge, $c_h/2m\omega_h$
μ	=	airfoil/air mass ratio, $m/\pi\rho b^2$
ξ	=	nondimensional plunge displacement, h/b
τ	=	nondimensional time, tV/b
$\bar{\omega}_\xi$	=	uncoupled frequency ratio, ω_h/ω_α

Received 24 November 2005; accepted for publication 20 October 2006.

*Adjunct Professor, Mechanical Engineering.
†Professor, Mechanical Engineering.

Introduction

AEROELASTIC systems are often modeled linearly to predict potentially unstable behavior. Conventional linear structural and aerodynamic models, however, are unable to predict phenomena such as limit-cycle oscillations (LCO) and chaos arising from aeroelastic nonlinearities. Nonlinearities in aeroelastic systems may arise from a number of sources, and may be mathematically complex to describe. The mathematical model of such a nonlinear system must be tested against experimental behavior to determine if it can successfully predict the relevant aspects of the nonlinear behavior. The literature contains a number of examples of mathematical modeling and numerical simulation of experimental nonlinear aeroelastic testing.

Hauenstein and Zara [1] compare numerically generated time histories to experimental results for a rigid, two-dimensional airfoil with freeplay stiffness nonlinearities in both the pitch and plunge degrees of freedom. The study focuses on sustained responses including limit-cycle oscillations, nonperiodic and chaotic behavior. The damping values in the analytical model were adjusted to match the airspeed at which sustained oscillations occurred for the analytical and experimental systems. The authors found that although the numerical simulation was able to predict the generic type of response (LCO, nonperiodic, or chaotic), it was inconsistent in its ability to quantitatively match the experimental behavior. They conclude that the influence of unmodeled system nonlinearities, probably damping, affected the experimental and analytical correlation.

O'Neil and Strganac [2] have also compared experimental and numerical results. Their study concerns the free response of a rigid, two-dimensional airfoil with a cubic stiffness nonlinearity in the pitch degree of freedom. Both viscous and Coulomb-type damping forces are included in the mathematical model. The aerodynamic forces are assumed to be linear and are modeled using quasi-steady aerodynamic theory. The model was used to study the limit-cycle behavior of the nonlinear system, and to predict the onset of divergent flutter for a number of linear system configurations. Some slight differences were noted between the predicted and measured flutter velocities and frequencies for the linear system. The nonlinear model was used to predict the onset of limit-cycle oscillations and to investigate the effect of initial conditions on the airspeed at which instabilities occur. The results of this study indicate the importance of modeling frictional forces in the structural equations, and they attribute differences between experimental measurements and numerical predictions to unmodeled nonlinearities in damping.

Sheta et al. [3] have done numerical modeling of experimental aeroelastic systems for the same experimental apparatus as O'Neil

and Strganac [2]. In their study, the mathematical structural model contains both viscous and Coulomb damping terms, and the hardening spring-type nonlinearity in pitch is modeled as a fifth-order polynomial. The aerodynamic forces are computed using a CFD-NASTRAN full Navier–Stokes solver to account for the possibility of viscosity effects, high angle of attack, vorticity evolution, and shedding. For the particular aeroelastic system under study, there is little variation in LCO frequency and amplitude over a large range of freestream velocities. Only nontransient, limit-cycle oscillations are considered and all of the cases presented are for an initial displacement in plunge only. The numerical model predicts values of frequency and amplitude of the limit-cycle motion that are in good agreement with the experimental results, especially for the pitch degree of freedom. This study compares six different combinations of structural and aerodynamic mathematical models for a limit-cycle oscillation at a specific airspeed. The authors show that the Theodorsen inviscid, unsteady analytical aerodynamic model can predict the occurrence of the limit-cycle motion, but predicts amplitudes in plunge that are 2.6 times the experimental values. They show that if viscous damping is not included in the structural model, the predicted limit-cycle amplitude in plunge is 2.25 times the measured value. Limit-cycle response is also simulated using a Euler (inviscid) flow solver, and the results are reasonably good, although the plunge motion amplitude is higher than that predicted using the Navier–Stokes solver. The authors conclude that it is important to model all of the aerodynamic and structural nonlinearities of the system, including the damping and viscous effects.

Tang and Dowell [4] have compared theoretical and experimental results for the free and forced response of a 2-degree-of-freedom helicopter blade model with a parabolic, cubic, or freeplay torsional stiffness nonlinearity. Their structural model does not include Coulomb damping, and the subsonic aerodynamics are modeled using the unsteady Theodorsen analytical model. For the free-response case with a freeplay nonlinearity, they use numerical simulations to investigate the relationship between limit-cycle amplitude and airspeed for a number of freeplay gap sizes. The numerical model is used to simulate a chaotic response at a particular airspeed. Experimental and numerical time histories and phase plane plots show similar behavior, and PSD diagrams obtained from the experimental and numerical data show good agreement. Numerical data for a parabolic nonlinearity predict limit-cycle motion, although the magnitudes of the amplitude and frequency estimates are slightly overestimated.

Conner et al. [5] have compared numerical and experimental results for a 3-degree-of-freedom system comprising a rigid, two-dimensional airfoil/flap system with a freeplay nonlinearity in the flap restoring moment. The structural model includes viscous damping but not Coulomb friction, and the subsonic aerodynamics are simulated using Theodorsen's model. For the linear case, there was a 15% difference in the predicted flutter speed between the mathematical model and the experimental system, which the authors attribute to nonlinear and three-dimensional aerodynamic effects not modeled in the equations of motion. For the nonlinear system, the amplitudes and frequencies of limit-cycle oscillations obtained from simulated and experimental data are compared for a large range of airspeeds. The numerical model can duplicate the qualitative behavior of the system for a number of freeplay gap sizes, including changes from low-frequency limit-cycle motion to nonperiodic motion and then to a high-frequency limit cycle. There were differences in the frequencies of oscillation between the numerical and experimental models, and the numerical model tended to overestimate the amplitude of the limit-cycle motion in the plunge degree of freedom. Numerical and experimental limit-cycle amplitudes in pitch and flap are in good agreement.

Tang et al. [6] model the same experimental data discussed in the preceding paragraph, but they use a reduced-order aerodynamic model based on Peters' finite state model [7]. The results obtained are similar to those obtained by Conner et al. [5] using a state-space representation of an approximation of Theodorsen's analytical aerodynamic model. In a continuation of this study, Tang et al. [8] use a describing function approach to analyze the nonlinear equations. They show that the airspeed for which limit-cycle oscillations can occur is independent of the size of the freeplay. They suggest that the minimum airspeed for which an LCO may occur, for any uncoupled frequency ratio, and for any freeplay size, corresponds to the minimum flutter velocity for the linear system without freeplay and with the frequency ratio allowed to assume the value that minimizes the flutter velocity. They also show that although an LCO may occur for any airspeed greater than this minimum flutter velocity, there is a minimum initial disturbance required to initiate limit-cycle motion.

The development of the analytical model described in the present paper is motivated by the experimental results of Marsden and Price [9]. The experiments were performed for a number of different freeplay sizes and a number of different frequency ratios. It was found that for this particular experimental system, the existence of LCO did in fact appear to depend on the freeplay size and the uncoupled frequency ratio. Although the analytical model of Tang et al. [8] demonstrates that there exists a single minimum airspeed for the potential onset of LCO in any particular aeroelastic system, the experimental results of Marsden and Price [9] suggest that there are other parameters that are important in determining the actual onset of the instability. One of these parameters is certainly the initial conditions, as it has been shown that at some airspeeds any small disturbance will initiate an LCO, whereas for other airspeeds a significant disturbance is required to produce the instability. In this study, a mathematical model is developed as a tool to better understand which parameters determine the occurrence of LCO. The model is developed based on the observation that it is within the first few oscillations of the transient response that the LCO is or is not established. The important parameters are therefore assumed to be those that determine the immediate, transient response of the system to an initial disturbance, and the model is built with the objective of accurately duplicating that response. The most influential structural and aerodynamic parameters are identified and included in the mathematical model, and simulated time-history data are compared with experimental records to validate the choice of parameters. The specific experimental wind-tunnel apparatus is modeled analytically, and the equations of motion are solved numerically to obtain simulated time-history data for the free response of a rigid airfoil to initial displacements in each of its 2 degrees of freedom.

Experimental Data

The experimental data used in this study are from a series of wind-tunnel experiments described in [9,10]. The experiments were performed on a rigid two-dimensional NACA 0012 wing section. The mounting system for the wing section is based on the original design by O'Neil and Strganac [2]. It enables the wing section to oscillate freely in pitch and plunge, with an adjustable restoring force and moment in the plunge and pitch degrees of freedom, respectively. A nonlinear mechanism is introduced in the pitch degree of freedom to allow for a pitching restoring moment freeplay region with adjustable parameters. The adjustable parameters are the size of the freeplay region, the restoring moment in the freeplay region, or preload, and the location of the freeplay region within the range of pitching motion of the wing section. Time-history data are obtained for the wing section free response to two different initial displacements in the plunge and pitch degrees of freedom, respectively, for a range of test airspeeds. Results are obtained for the linear and three nonlinear system configurations and for a range of airspeeds between zero and the linear flutter speed. The nonlinear systems correspond to freeplay sizes of 0.37, 0.69, and 1.54 degrees of total freeplay.

The response data of the experimental system may be divided into three groups by qualitative observation of the time history. The responses are classified as damped as shown in Fig. 3; limit-cycle flutter, or LCO, as shown in Fig. 14; or combined damped and limit-cycle response as shown in Fig. 12 (the figures will be discussed later in this paper). The mixed damped and LCO type of response is thought to be a result of dry friction in the system damping out an

LCO. The experimental data used for comparison in this numerical study were all obtained for a plunge/pitch frequency ratio, ω_h/ω_α, of 0.366.

Modeling the Airfoil Section

The symmetric, two-dimensional airfoil section shown in Fig. 1 is a modified version of the typical section airfoil model often used in the study of aeroelastic problems. The typical section is particularly applicable to the study of binary flutter involving coupling between the bending and torsional motions of an aircraft wing or tail surface. The rigid airfoil is mounted by torsional and translational springs attached at the elastic axis, or shear center of the section, and is free to move in both the plunge and pitch directions. The plunge deflection h is measured positive downward and the pitch angle about the elastic axis α is positive for the airfoil leading edge up.

The mass distribution of the airfoil section model differs from that normally used for this type of numerical study in that it has been "customized" to more adequately represent the dynamic behavior of the experimental system. In the experimental system, the mass in the pitch and the plunge degrees of freedom are not the same and it is necessary to define two distinct masses for the airfoil section, each of which is associated with one of the two degrees of freedom. The two masses are designated as the "moving mass in plunge" and the "moving mass in pitch." For the experimental section modeled in this study, the moving mass in plunge is six times greater than the moving mass in pitch. In addition to the two different masses in pitch and plunge, the distribution of mass in the airfoil section is defined as two separate point masses rather than as a single mass. The experimental section is constructed from a lightweight composite material bonded to an aluminum axle, resulting in a large mass at the center of rotation that cannot be modeled as a single mass concentrated at a single point of the airfoil section. The mass of the airfoil section is therefore separated into two concentrated masses: one representing the aluminum axle and centered at the elastic axis, and the other representing the mass of the airfoil section without the axle and located at the center of mass of the airfoil section. The total mass of the system is divided into three parts, where m_1 represents the additional mass in the plunge degree of freedom peculiar to the experimental apparatus being modeled. The mass m_2 represents the mass of the airfoil section and pitching mechanism, centered on the elastic axis of the airfoil model. This concentrated mass is located at the elastic axis and thus contributes to the moment of inertia in pitch, but does not influence the coupling between the two degrees-of-freedom. The mass of the body of the airfoil section is m_3 and has its center of mass located at a distance bx_α from the elastic axis. The mass m_3 is the only mass that contributes to the coupling between the pitch and plunge degrees of freedom. The moving mass in plunge is $m_h = m_1 + m_2 + m_3$, and the moment of inertia about the elastic axis is I_α, based on the moving mass in pitch, $m_p = m_2 + m_3$.

Equations of Motion

Taking into account the distribution of mass described in the preceding section, the kinetic energy of the moving two-dimensional airfoil may be written as

$$T = \frac{1}{2} m_h \dot{h}^2 + m_3 b x_\alpha \dot{\alpha}\, \dot{h} + \frac{1}{2} I_\alpha \dot{\alpha}^2$$

Applying Lagrange's equations, the equations of motion may be expressed as shown in Eqs. (1) and (2).

$$m_h \ddot{h}(t) + m_3 b x_\alpha \ddot{\alpha}(t) + C_h \dot{h}(t) + \bar{F}(h) = P(t) \tag{1}$$

$$m_3 b x_\alpha \ddot{h}(t) + I_\alpha \ddot{\alpha}(t) + C_\alpha \dot{\alpha}(t) + \bar{M}(\alpha) = R(t) \tag{2}$$

In the preceding equations, C_h and C_α are the viscous damping factors and $P(t)$ and $R(t)$ are the externally applied forces and moments in plunge and pitch, respectively. For the linear system,

$$\bar{F}(h) = K_h h \qquad \bar{M}(\alpha) = K_\alpha \alpha = I_\alpha \omega_\alpha^2 \alpha$$

For the nonlinear system, the restoring moment in the pitch degree of freedom, $M(\alpha)$, is shown in Fig. 2. This type of nonlinearity is often referred to as bilinear or freeplay and is characterized by a discontinuity in the restoring moment over a limited range of motion. The parameters describing the nonlinearity are its length δ, the pitch angle at which the discontinuity is located within the range of motion of the airfoil α_f, and the restoring moment in the freeplay region m_0. The freeplay nonlinearity shown in Fig. 2 is modeled mathematically as follows:

$$M(\alpha) = \begin{cases} m_0 + \alpha - \alpha_f & \text{for } \alpha < \alpha_f \\ m_0 & \text{for } \alpha_f \le \alpha \le \alpha_f + \delta \\ m_0 + \alpha - \alpha_f - \delta & \text{for } \alpha_f + \delta < \alpha \end{cases}$$

The appropriate initial conditions in pitch and plunge can be used with Eqs. (1) and (2) to obtain simulated time histories of the experimental airfoil's structural response to an initial displacement.

When the airspeed in the wind tunnel is not zero, the aerodynamic terms are obtained from Fung [11]. The full equations in the plunge and pitch degrees of freedom, respectively, are shown as follows in nondimensional form:

$$\xi''(\tau) + \frac{m_3}{m_h} x_\alpha \alpha''(\tau) + 2\zeta_\xi \frac{\bar{\omega}_\xi}{U} \xi'(\tau) + \left(\frac{\bar{\omega}_\xi}{U}\right)^2 \xi(\tau) = F_\xi\left(\frac{\xi'}{|\xi'|}\right) - \frac{1}{\mu}[\xi''(\tau) - a_h \alpha''(\tau) + \alpha'(\tau) + 2XTM] \tag{3}$$

and

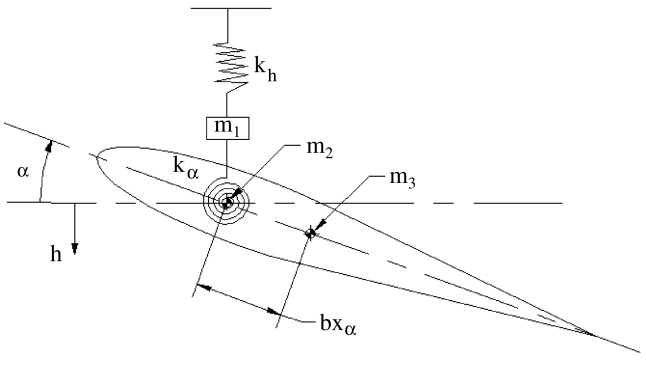

Fig. 1 Airfoil section model.

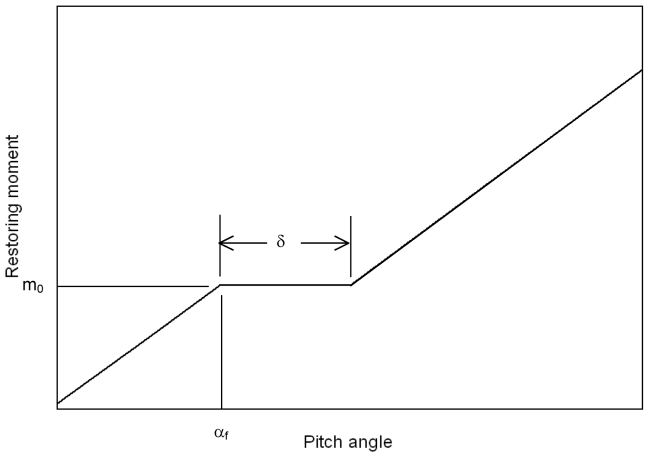

Fig. 2 Schematic of nonlinear restoring moment in pitch.

$$\frac{m_3 b^2 x_\alpha}{I_\alpha}\xi''(\tau) + \alpha''(\tau) + 2\zeta_\alpha \frac{1}{U}\alpha'(\tau) + \frac{1}{U^2}M[\alpha(\tau)]$$
$$= F_\alpha\left(\frac{\alpha'}{|\alpha'|}\right) + \frac{1}{\mu r_\alpha^2}[a_h\xi''(\tau) - (\tfrac{1}{8} + a_h^2)\alpha''(\tau)$$
$$- (\tfrac{1}{2} - a_h)\alpha'(\tau) + 2(\tfrac{1}{2} + a_h)XTM] \quad (4)$$

where the expressions XTM, C_1, and $\lambda(\sigma)$ are given in the Appendix.

The aerodynamic model used in Eqs. (3) and (4) is based on Theodorsen's inviscid, unsteady equations for subsonic flow where Wagner's function $\phi(\tau)$ has been replaced by the approximation given by Jones [12]:

$$\phi(\tau) = 1 - 0.165e^{-0.0455\tau} - 0.335e^{-0.3\tau}$$

There is considerable friction damping in the experimental system that cannot be adequately modeled by the viscous damping terms in the preceding equations. For this reason, two structural frictional forces are included in the right-hand sides of Eqs. (3) and (4). The friction forces are modeled as constant terms, F_α and F_ξ, that act opposite to the direction of motion of the airfoil in their respective degree of freedom. The magnitude of F_α and F_ξ are determined by matching the experimental and simulated time histories, as will be discussed in the next section.

Time-history solutions to the nonlinear integro-differential equations, Eqs. (3) and (4), are obtained using a finite difference method developed by Houbolt [13]. The method has been used to obtain solutions for unforced aeroelastic oscillations by Lee and Desrochers [14], Price et al. [15,16], and Marsden [10]. Houbolt's finite difference method was chosen for the numerical integration of Eqs. (1–4) because it can accommodate the presence of three discontinuities in the differential equations; the freeplay in the pitch degree of freedom restoring moment and the frictional forces which are proportional to the direction of motion in both the pitch and plunge degrees of freedom. The method results in a system of equations which may be solved algebraically to yield the displacements in plunge and in pitch at time $t + \delta t$ in terms of the displacement values at times t, $t - \delta t$, and $t - 2\delta t$. Details are given in [10].

Equations (3) and (4) are solved numerically at increments of nondimensional time τ to produce time histories of the airfoil section response to initial displacements in the pitch and plunge degrees of freedom. The nondimensional time step used is 0.007, and was tested to confirm convergence. The physical parameters for the airfoil section are shown in Table 1. The effective spring constants in pitch and plunge were measured directly, and the moving mass in plunge and pitch, as well as the moment of inertia in pitch were determined by matching experimental and theoretical results for the wind-off condition as will be described later in this paper. The aerodynamic parameters such as wind velocity and air density are taken from the experimental records. The initial displacements in pitch and plunge for each simulation are from the measured experimental data, and the initial airfoil velocity is assumed to be zero for all cases. Simulations are done over the entire range of airspeeds tested experimentally, for the linear system and for three different sizes of freeplay in the restoring moment in pitch.

Table 1 Wing section physical properties

Moving mass in plunge, m_h	2.38 kg
Moving mass in pitch, m_α	0.393 kg
Wing section chord	0.203 m
Wing section span	0.572 m
Distance from elastic axis to midchord	0.031 m
Moment of inertia, I_α	0.0028 kg · m^2
Distance from midchord to airfoil center of moving mass in pitch	0.032 m
K_p, effective spring constant in plunge	3231 N/m
K_α, effective torsional spring constant	35.4 m · N/rad

Results: Linear Structural Model

The simulation of the experimental results was done in stages to validate in sequence the linear structural model, the nonlinear structural model, and finally, the aerodynamic model for both the linear and the nonlinear cases. Figure 3 shows the airfoil section structural response, for the wind-off condition, to an initial displacement in pitch. These responses are typical of the initial displacements in pitch and plunge (not shown) that were used to obtain several of the airfoil section physical properties listed in Table 1, as well as to validate the numerical model of the structural system with no aerodynamics.

Matching the responses in pitch and plunge, as well as the induced displacements in each degree of freedom was used to establish a number of structural parameters. The moment of inertia in pitch I_α was calculated using Fig. 3a, which shows the airfoil response in the pitch degree of freedom to an initial displacement in pitch of 5.0 deg, for the wind-off condition. Using the experimentally measured spring stiffness in pitch, the moment of inertia in the pitch degree of freedom was determined by matching the simulated and experimental time histories as shown in the figure. A similar procedure was used to determine the moving mass in plunge m_h using the experimentally measured plunge degree-of-freedom stiffness and the time-history data for the airfoil section response to an initial displacement in plunge. Figure 3b shows the time-history data for motion in the plunge degree of freedom induced by an initial displacement in pitch. Matching the simulated and experimental time histories for this case and the corresponding motion in pitch induced by an initial displacement in the plunge degree of freedom (not shown) allows the validation of the estimate for the mass of the airfoil section without the aluminum axle m_3, as well as the distance from the elastic axis to the location of the mass bx_α. Matching the numerical and experimental data for all of the preceding cases also validates the values used to represent the frictional forces included in the mathematical model. The nondimensional values obtained for the frictional forces in plunge and pitch are given next. These values are

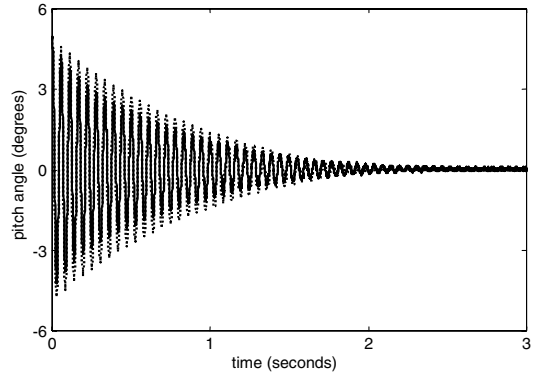

a) Pitch response

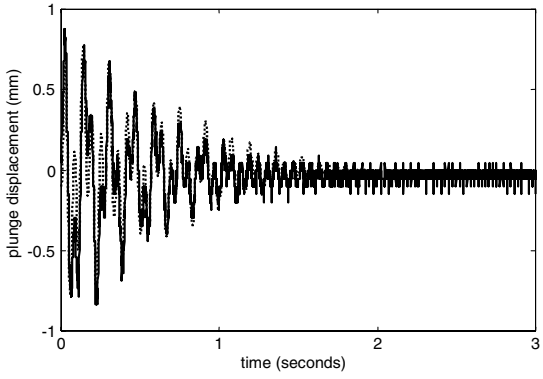

b) Plunge response induced by pitch displacement

Fig. 3 Airfoil linear response to an initial displacement of 5.0 deg in pitch at 0.0 m/s: solid line, experimental data; dotted line, numerical simulation.

used for all the numerical simulations presented in this paper, for both the linear and the nonlinear systems.

$$F_\xi = 0.18 \qquad F_\alpha = 0.0005$$

The ability of the numerical model to match the experimental behavior is very good, although the numerical model tends to slightly overpredict the pitching motion amplitudes for the initial transient response shown in Fig. 3a.

The values obtained for the frictional forces by matching experimental and simulated data were validated with respect to the balance between viscous and Coulomb damping forces. This was done by calculating the peak amplitude decrement associated with the assumed frictional force and subtracting that value from the actual decrement measured experimentally. The resultant experimental damping values (total decrement less friction damping) were then plotted on a logarithmic decrement plot. The ability of the points to define a straight line was used to verify that the remaining decrement was a result of purely viscous damping.

Results: Nonlinear Structural Model

Once the structural parameters of the linear system were established and validated, the model was expanded to include the physical parameters of the nonlinear system with freeplay in the pitch degree-of-freedom restoring moment. The free-response time histories to an initial displacement in pitch for the smallest freeplay size, 0.37 deg, are shown in Fig. 4. Figure 4a compares the simulated and experimental data for the airfoil pitch response to an initial displacement in pitch. Similar responses to an initial displacement in the plunge degree of freedom are not shown. The simulated data were obtained using the identical physical parameters employed previously for the linear system. It was during this phase of the model construction that the influence of additional frictional forces in the experimental freeplay mechanism became evident. If the pitch response to an initial displacement in pitch shown in Fig. 3a (for the linear system) is compared to the equivalent response of the nonlinear system shown in Fig. 4a, a dramatic increase in damping is evident in the nonlinear response. The same difference in damping is not seen in the plunge response to an initial displacement in plunge (not shown). These results imply the presence of an additional damping force only in the pitch degree of freedom and only in the nonlinear system, and simulations based on Eqs. (3) and (4) were unable to account for the increased damping. As a result of an investigation of the experimental apparatus, the model was modified to incorporate additional Coulomb and viscous frictional forces. The additional forces act only in the freeplay region of the pitching motion, and are a result of the friction present in the experimental freeplay mechanism. The numerical model of the aeroelastic system was modified to include these additional forces and the results for the pitch degree of freedom are as seen in Fig. 4. The numerical model with the additional forces in freeplay is capable of reproducing the experimental behavior with a high degree of accuracy. Numerical results match experimental data for initial displacements in both pitch and plunge, as well as the transient induced responses in the opposite degrees of freedom, as exemplified by Fig. 4b for the plunge response to an initial displacement in pitch.

The introduction of additional freeplay damping forces in the numerical model is validated by comparing the results for the other two freeplay sizes, an example of which is shown in Fig. 5 for the 0.69-deg freeplay system. In all cases, the rather dramatic increase in damping for an initial displacement in pitch as the freeplay size is increased can be accounted for by the presence of the additional damping forces in the freeplay mechanism, where the same magnitude of force is used in all of the simulations. As the freeplay size is increased, the influence of the freeplay forces becomes increasingly evident, and in all cases the mathematical model successfully models the behavior of the nonlinear systems. Additional confidence in the validity of the "friction in freeplay" assumption may be gained by considering the very small amplitudes of pitch response induced by the mass coupling to an initial

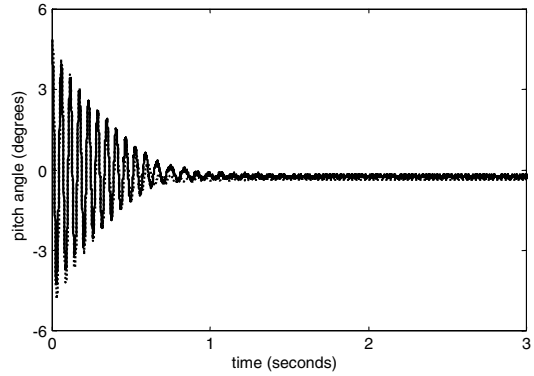

a) Pitch response

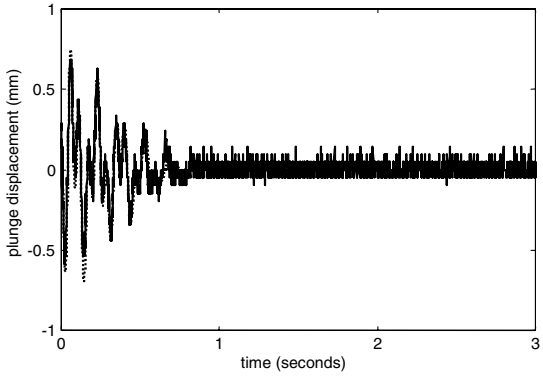

b) Plunge response induced by pitch displacement

Fig. 4 Airfoil nonlinear response to an initial displacement of 4.6 deg in pitch for 0.37-deg freeplay at 0.0 m/s: solid line, experimental data; dotted line, numerical simulation.

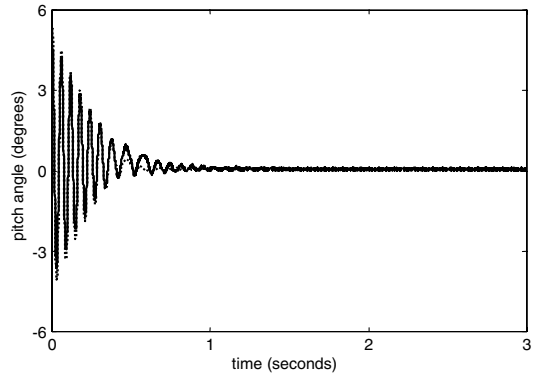

a) Pitch response

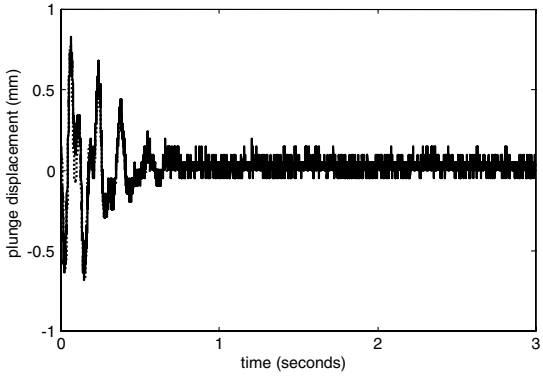

b) Plunge response induced by pitch displacement

Fig. 5 Airfoil nonlinear response to an initial displacement of 5.3 deg in pitch for 0.69-deg freeplay at 0.0 m/s: solid line, experimental data; dotted line, numerical simulation.

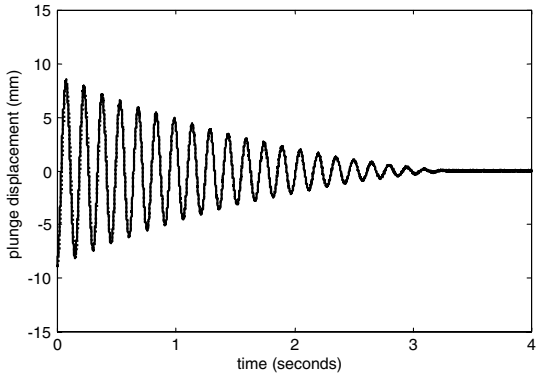

a) Plunge response

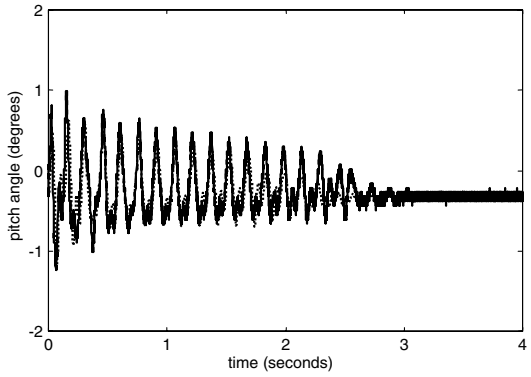

b) Pitch response induced by plunge displacement

Fig. 6 Airfoil nonlinear response to an initial displacement of −8.7 mm in plunge for 0.37-deg freeplay at 0.0 m/s: solid line, experimental data; dotted line, numerical simulation.

displacement in the plunge degree of freedom, as shown in Fig. 6b. Figure 6a shows the response in plunge to an initial displacement in plunge for a freeplay size of 0.37 deg, and Fig. 6b shows the induced response in pitch. Other cases for the other freeplay sizes were tested but are not shown here. For all the cases, the freeplay size, the freeplay friction, and the mass coupling between the two degrees of freedom overwhelmingly determine the response, and the agreement between the model and the experiment is excellent, as shown in Fig. 6b. In addition, the model can predict the extremely small amplitudes (less than 1 mm) of induced plunge response to an initial displacement in pitch as shown in Figs. 4b and 5b. Modeling the linear and nonlinear systems at the wind-off condition without any aerodynamics validates the mathematical model of the physical experimental apparatus, including the freeplay nonlinearity.

Results: Linear and Nonlinear Aeroelastic Models

Once the structural model was finalized, the unsteady aerodynamic model was added to the linear system. The simulated responses for the linear system were compared to the experimental results for nine different airspeeds ranging from 0 to 78% of the linear flutter speed. Figures 7 and 8 compare the simulated and experimental responses for the linear system at 42 and 73% of the flutter speed, respectively. A number of characteristics typical of aeroelastic systems can be seen in these figures. Figure 7a, when compared to Fig. 3a demonstrates how the response to an initial displacement in pitch becomes increasingly damped, and the response frequency decreases, as the airspeed is increased toward the flutter speed. The corresponding response in plunge induced by an initial displacement in pitch, shown in Fig. 7b, when compared to Fig. 3b does not show the same damping trend, and shows a dramatic increase in plunge amplitude as the airspeed is increased. This increase in plunge amplitude with airspeed is a result of the static aerodynamic load, and demonstrates the importance of including the steady-state aerodynamics in the model if the transient response of

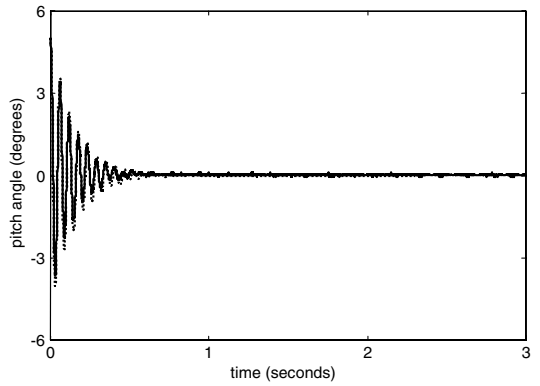

a) Pitch response

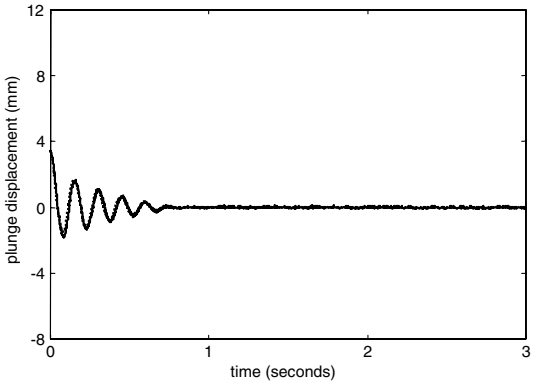

b) Plunge response induced by pitch displacement

Fig. 7 Airfoil linear response to an initial displacement of 5.0 deg in pitch at 21.6 m/s or 42% of the linear flutter speed: solid line, experimental data; dotted line, numerical simulation.

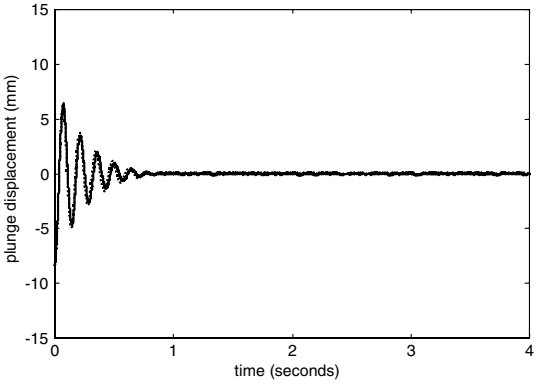

a) Plunge response

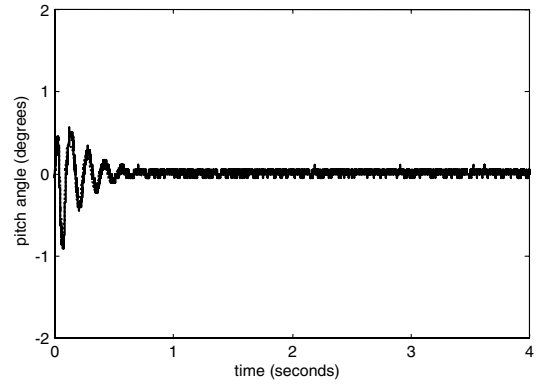

b) Pitch response induced by plunge displacement

Fig. 8 Airfoil linear response to an initial displacement of −8.0 mm in plunge at 37.9 m/s or 73% of the linear flutter speed: solid line, experimental data; dotted line, numerical simulation.

the airfoil is of interest. The airfoil response to an initial displacement in plunge also becomes increasingly damped with airspeed, whereas the frequency of the oscillations increases. Figure 8a shows the airfoil section response in the plunge degree of freedom to an initial displacement in plunge at 73% of the linear flutter speed. The corresponding induced motion in the pitch degree of freedom is shown in Fig. 8b. In general, the responses in pitch to initial displacements in plunge do not increase in amplitude with increasing airspeed as was the case for the response in plunge to a displacement in pitch, and the damping can be seen to increase as the flutter speed is approached. The simulated data accurately represent all of these behaviors of the aeroelastic system, demonstrating that the model is capable of reproducing the transient, damped response of the linear aeroelastic system to initial displacements in both the pitch and plunge degrees of freedom over a large range of airspeeds between zero and the linear flutter speed.

Finally, the nonlinear structural equations were combined with the aerodynamic model to simulate the aeroelastic behavior of the three nonlinear system configurations. Figures 9–14 are examples of the results obtained for the smallest freeplay length, 0.37 deg. Figures 9 and 10 show the nonlinear system response to initial displacements in pitch and plunge, respectively. These figures are typical examples of a nonlinear response that appears to be linear in both the damped response as seen in Figs. 9a and 10a, and in the coupled response as seen in Figs. 9b and 10b. Figures 11 and 12 show the damped limit-cycle type of response. For the case of an initial displacement in pitch, Fig. 11, the numerical model predicts the damped-type limit cycle, but overestimates the number of cycles of motion before the damping takes effect. This is particularly evident in Fig. 11b, where, in addition, the numerical model has overestimated the amplitude of the limit-cycle motion in the plunge degree of freedom (although, with reference to the scale of the figure, the overestimate is quite small, at less than 0.5 mm). The same system, under the same conditions, but subjected to an initial displacement in plunge,

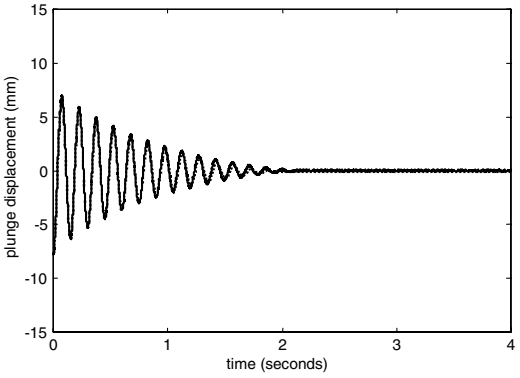

a) Plunge response

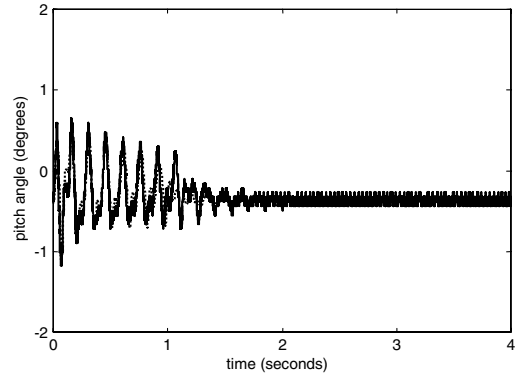

b) Pitch response induced by plunge displacement

Fig. 10 Airfoil nonlinear response to an initial displacement of −7.8 mm in plunge at 12.0 m/s or 23% of the linear flutter speed, for a freeplay size of 0.37 deg: solid line, experimental data; dotted line, numerical simulation.

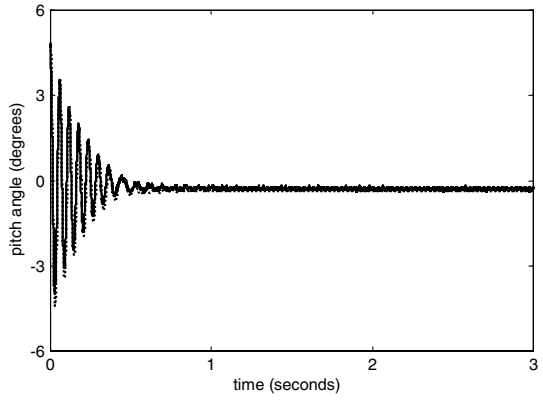

a) Pitch response

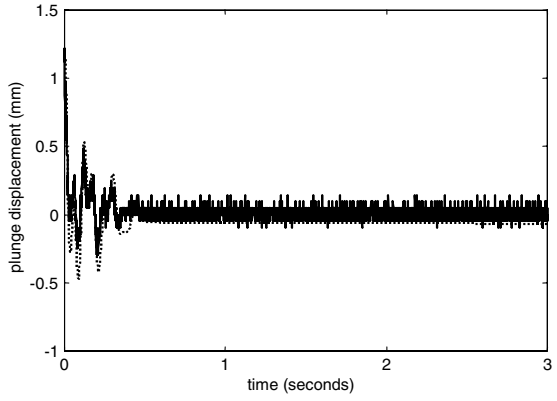

b) Plunge response induced by pitch displacement

Fig. 9 Airfoil nonlinear response to an initial displacement of 4.6 deg in pitch at 12.0 m/s or 23% of the linear flutter speed, for a freeplay size of 0.37 deg: solid line, experimental data; dotted line, numerical simulation.

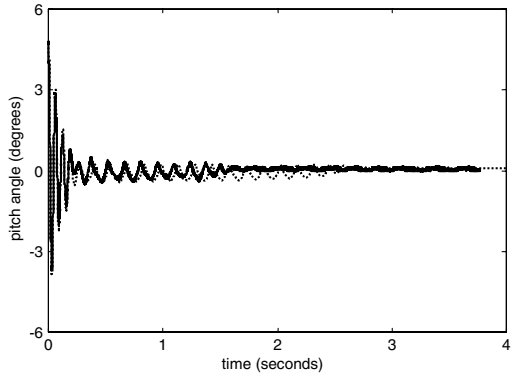

a) Pitch response

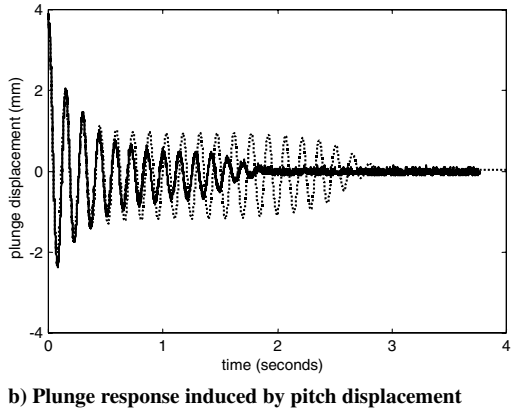

b) Plunge response induced by pitch displacement

Fig. 11 Airfoil nonlinear response to an initial displacement of 4.6 deg in pitch at 23.4 m/s or 43% of the linear flutter speed, for a freeplay size of 0.37 deg; solid line, experimental data; dotted line, numerical simulation.

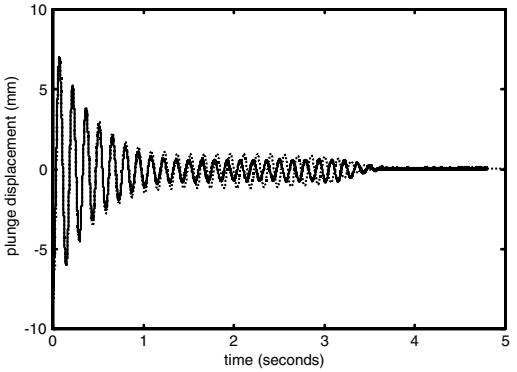

a) Plunge response

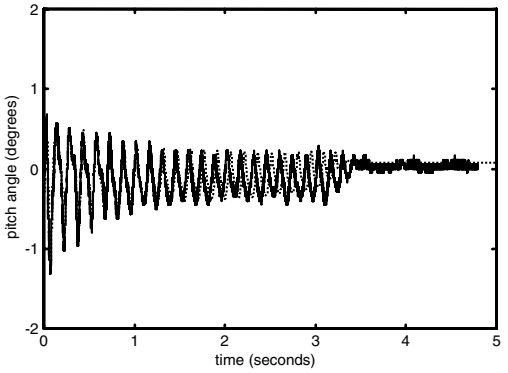

b) Pitch response induced by plunge displacement

Fig. 12 Airfoil nonlinear response to an initial displacement of −7.8 mm in plunge at 23.4 m/s or 43% of the linear flutter speed, for a freeplay size of 0.37 deg: solid line, experimental data; dotted line, numerical simulation.

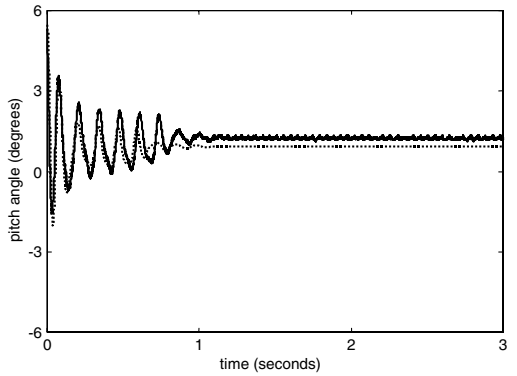

a) Pitch response

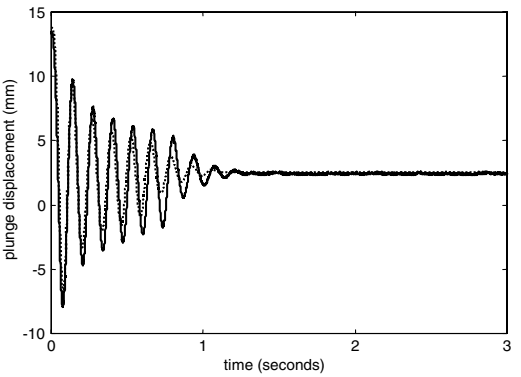

b) Plunge response induced by pitch displacement

Fig. 13 Airfoil nonlinear response to an initial displacement of 4.6 deg in pitch at 42.1 m/s or 78% of the linear flutter speed, for a freeplay size of 0.37 deg: solid line, experimental data; dotted line, numerical simulation.

responds as shown in Fig. 12. In this case, the numerical model predicts the correct number of cycles before the limit-cycle motion is damped, although a small overestimate in amplitude in plunge can be seen. It is interesting to note that the model predicts the correct frequency for the initial transient, damped motion shown in Fig. 12a, but underestimates the frequency of the subsequent limit-cycle oscillation. The induced limit-cycle motion in pitch, shown in Fig. 12b, is very accurately duplicated by the numerical data, although the frequency of the simulated limit-cycle motion is slightly lower than for the experimental results. Figures 13 and 14 are examples of the third type of response seen during the experiments, the fully developed limit-cycle oscillation. The response to an initial displacement in pitch, shown in Figs. 13a and 13b, contains only two or three limit cycles before damping to zero, but the response to an initial displacement in plunge, shown in Figs. 14a and 14b, is a fully developed limit-cycle type of response. The numerical model is able to duplicate both of these responses with a good degree of accuracy, although in the case of Figs. 14a and 14b, the frequency of the limit-cycle oscillations is slightly higher for the simulation compared to the experimental data.

Three examples for the other two, larger freeplay sizes are shown in Figs. 15 and 16. Figure 15 shows the nonlinear system response to an initial displacement in pitch for the 0.69-deg gap at 30% of the linear flutter speed. In this case, the response is apparently a damped, or linear-type response, except that there is an abrupt and dramatic change in frequency during the fourth cycle of oscillation. This type of response is typical of the nonlinear system with freeplay, and the numerical model duplicates it very well. The same system responds to an initial displacement in plunge is shown in Fig. 16. In this case, the plunge response shown in Fig. 16a, and the corresponding pitch displacements shown in Fig. 16b are apparently linear, and the nonlinear behavior evident in the pitch response of Fig. 15 is not observed. Figures 17 and 18 are typical examples of full limit-cycle responses to initial displacements in pitch and plunge, respectively, for the 0.69-deg freeplay at 66% of the linear flutter speed. In both of

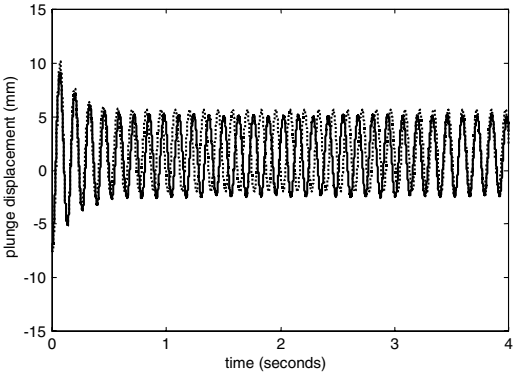

a) Plunge response

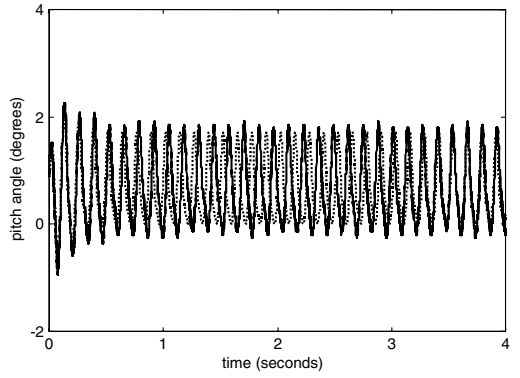

b) Pitch response induced by plunge displacement

Fig. 14 Airfoil nonlinear response to an initial displacement of −7.8 mm in plunge at 42.1 m/s or 78% of the linear flutter speed, for a freeplay size of 0.37 deg: solid line, experimental data; dotted line, numerical simulation.

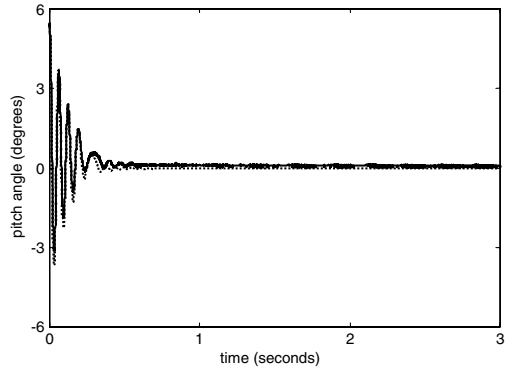

a) Pitch response

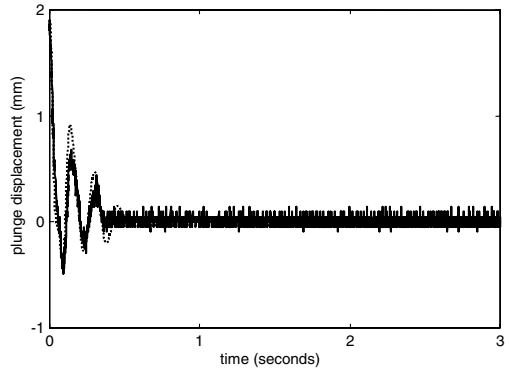

b) Plunge response induced by pitch displacement

Fig. 15 Airfoil nonlinear response to an initial displacement of 5.3 deg in pitch at 15.7 m/s or 30% of the linear flutter speed, for a freeplay size of 0.69 deg: solid line, experimental data; dotted line, numerical simulation.

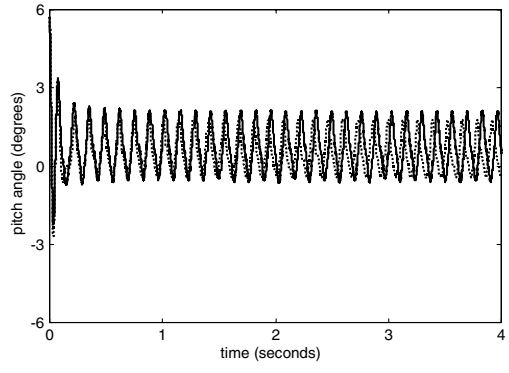

a) Pitch response

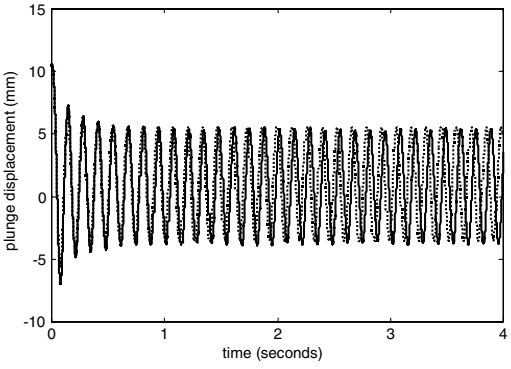

b) Plunge response induced by pitch displacement

Fig. 17 Airfoil nonlinear response to an initial displacement of 5.6 deg in pitch at 35.7 m/s or 66% of the linear flutter speed, for a freeplay size of 0.69 deg: solid line, experimental data; dotted line, numerical simulation.

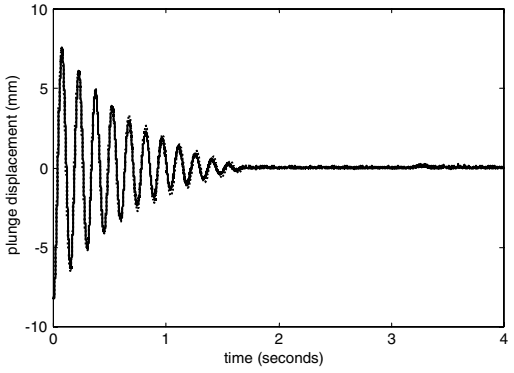

a) Plunge response

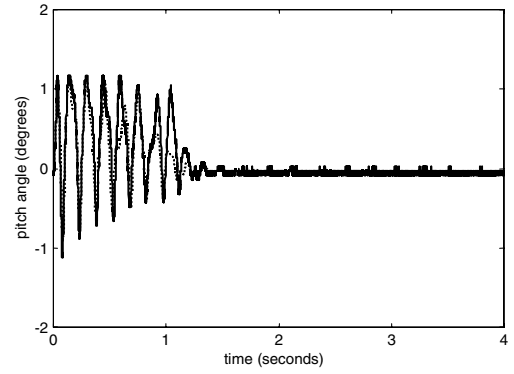

b) Pitch response induced by plunge displacement

Fig. 16 Airfoil nonlinear response to an initial displacement of −8.2 mm in plunge at 15.7 m/s or 30% of the linear flutter speed, for a freeplay size of 0.69 deg: solid line, experimental data; dotted line, numerical simulation.

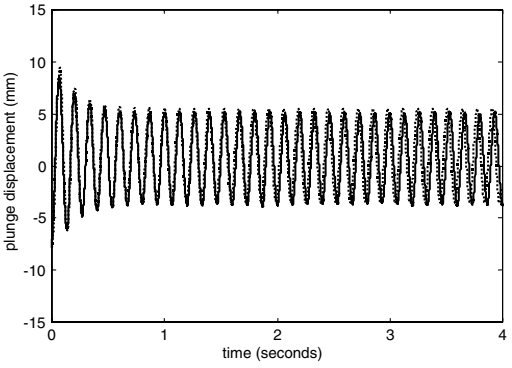

a) Plunge response

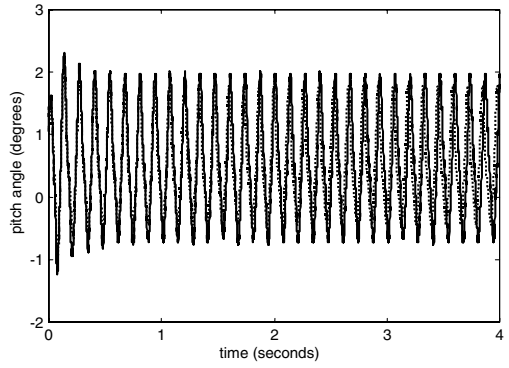

b) Pitch response induced by plunge displacement

Fig. 18 Airfoil nonlinear response to an initial displacement of −7.7 mm in plunge at 35.7 m/s or 66% of the linear flutter speed, for a freeplay size of 0.69 deg: solid line, experimental data; dotted line, numerical simulation.

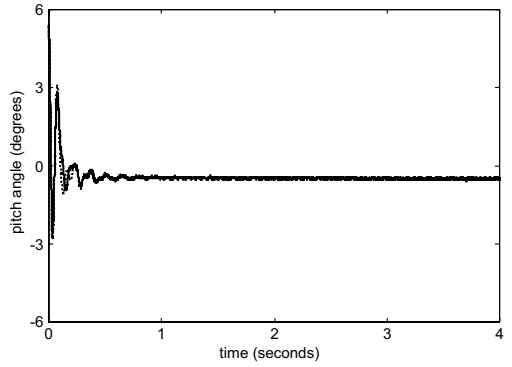

a) Pitch response

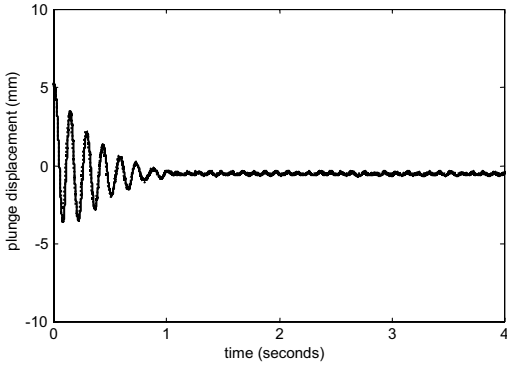

b) Plunge response induced by pitch displacement

Fig. 19 Airfoil nonlinear response to an initial displacement of 5.3 deg in pitch at 26.7 m/s or 49% of the linear flutter speed, for a freeplay size of 1.54 deg: solid line, experimental data; dotted line, numerical simulation.

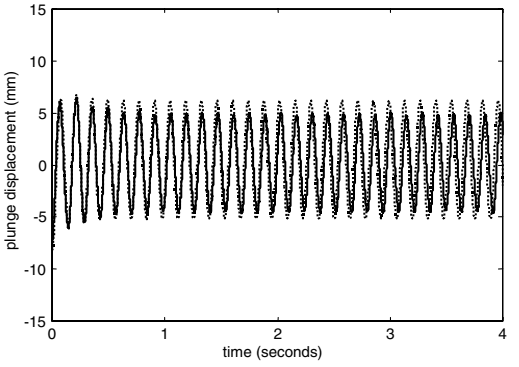

a) Plunge response

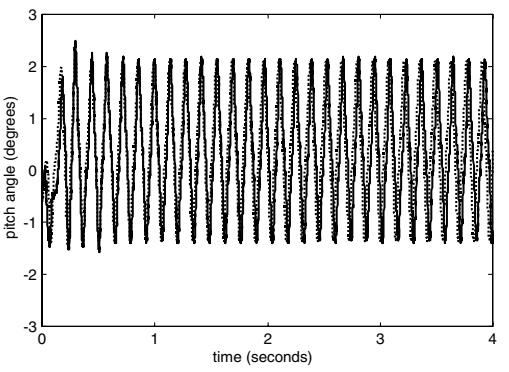

b) Pitch response induced by plunge displacement

Fig. 20 Airfoil nonlinear response to an initial displacement of −7.7 mm in plunge at 26.7 m/s or 49% of the linear flutter speed, for a freeplay size of 1.54 deg: solid line, experimental data; dotted line, numerical simulation.

these figures, the experimental behavior in pitch and plunge is quite accurately modeled by the numerical data. The final example, shown in Figs. 19 and 20, is for the largest freeplay size, or 1.54 deg, at 49% of the linear flutter speed, and is a case where an initial displacement in pitch results in a damped response, whereas an initial displacement in plunge produces a fully developed limit-cycle motion. The simulated data is again able to match the experimental curves for the largest gap size.

Conclusions

Aeroelastic systems containing discontinuous, freeplay-type nonlinearities can exhibit unstable, limit-cycle responses at airspeeds well below the divergent flutter speed predicted by the linear theory. It has been shown analytically [8] that the range of airspeeds for which these LCOs can occur is a function of the system parameters, but is independent of the freeplay size and the system frequency ratio. Physical aeroelastic systems, however, do not always behave in an unstable manner, even at airspeeds where an LCO response can be shown analytically to be possible. In this study, an experimental system that demonstrates a number of stable and unstable linear and nonlinear responses to an initial disturbance has been modeled mathematically. The study identifies several physical parameters that must be modeled to duplicate the experimental response to a high degree of accuracy. It was found that the most important elements in terms of correctly predicting the transient behavior of the airfoil section response were 1) the unsteady aerodynamic terms, 2) the steady-state aerodynamic forces, 3) the frictional forces, and 4) the mass distribution.

The model successfully predicts the transient behavior of the airfoil section for the linear and three nonlinear experimental cases over a large range of airspeeds, and correctly identifies the onset of limit-cycle instabilities. The model is, however, unable to precisely duplicate the frequency and amplitude of the LCO motion: a result that supports previous studies [3] where it has been shown that highly complex Navier–Stokes solvers are necessary to accurately model the frequencies and amplitudes of limit-cycle oscillations. On the other hand, the results suggest that the onset of LCO may be predicted if the transient response of the system can be accurately modeled, and that the transient response may be duplicated using a much simpler linear, unsteady aerodynamic model, provided that the important physical parameters of the system are identified and included in the model.

Appendix: Aerodynamic Coefficients

$$XTM = C_1\phi(\tau) + \int_0^\tau \lambda(\sigma)\phi(\tau-\sigma)\,\mathrm{d}\sigma$$

$$C_1 = \xi'(0) + (\tfrac{1}{2} - a_h)\alpha'(0) + \alpha(0)$$

$$\lambda(\sigma) = \xi''(\sigma) + (\tfrac{1}{2} - a_h)\alpha''(\sigma) + \alpha'(\sigma)$$

Acknowledgment

The authors gratefully acknowledge B. H. K. Lee of the National Research Council Aerospace Institute for the loan of the wind-tunnel section, without which the experimental portion of this study could not have been accomplished.

References

[1] Hauenstein, A. J., and Zara, J. A., "Chaotic and Nonlinear Dynamic Response of Aerosurfaces with Structural Nonlinearities," AIAA Paper 92-2547-CP, 1992, pp. 2367–2375.

[2] O'Neil, T., and Strganac, T. W., "Aeroelastic Response of a Rigid Wing Supported by Nonlinear Springs," *Journal of Aircraft*, Vol. 35, No. 4, 1998, pp. 616–622.

[3] Sheta, E. F., Harrand, V. J., Thompson, D. E., and Strganac, T. W., "Computational and Experimental Investigation of Limit Cycle Oscillations of Nonlinear Aeroelastic Systems," *Journal of Aircraft*, Vol. 39, No. 1, 2002, pp. 133–141.

[4] Tang, D. M., and Dowell, E. H., "Comparison of Theory and Experiment for Non-Linear Flutter and Stall Response of a Helicopter Blade," *Journal of Sound and Vibration*, Vol. 165, No. 2, 1993, pp. 251–276.

[5] Conner, M. D., Tang, D. M., Dowell, E. H., and Virgin, L. N., "Nonlinear Behaviour of a Typical Airfoil Section with Control Surface Freeplay: A Numerical and Experimental Study," *Journal of Fluids and Structures*, Vol. 11, No. 1, 1997, pp. 89–109.

[6] Tang, D., Conner, M. D., and Dowell, E. H., "Reduced-Order Aerodynamic Model and its Application to a Nonlinear Aeroelastic System," *Journal of Aircraft*, Vol. 35, No. 2, 1998, pp. 332–338.

[7] Peters, D. A., and Cao, W. M., "Finite State Induced Flow Models, Part 1: Two-Dimensional Thin Airfoil," *Journal of Aircraft*, Vol. 32, No. 2, 1995, pp. 313–322.

[8] Tang, D. M., Dowell, E. H., and Virgin, L. N., "Limit Cycle Behaviour of an Airfoil with a Control Surface," *Journal of Fluids and Structures*, Vol. 12, No. 7, 1998, pp. 839–858.

[9] Marsden, C. C., and Price, S. J., "The Aeroelastic Response of a Wing Section with a Structural Freeplay Nonlinearity: An Experimental Investigation," *Journal of Fluids and Structures*, Vol. 21, No. 3, 2005, pp. 257–276.

[10] Marsden, C., "An Experimental and Analytical Investigation of the Nonlinear Behaviour and Modal Analysis of a Structurally Nonlinear, Two-Dimensional Airfoil in Subsonic Flow," Ph.D. Dissertation, Mechanical Engineering Dept., McGill Univ., Montréal, Québec, Canada, 2005.

[11] Fung, Y. C., *An Introduction to the Theory of Aeroelasticity*, John Wiley, New York, 1955.

[12] Jones, W. P., "Summary of Formulae and Notations Used in Two-dimensional Derivative Theory," British Aeronautical Research Committee, Report and Memorandum 1958, London, 1942.

[13] Houbolt, J. C., "A Recurrence Matrix Solution for the Dynamic Response of Elastic Aircraft," *Journal of the Aeronautical Sciences*, Vol. 17, Sept. 1950, pp. 540–550.

[14] Lee, B. H. K., and Desrochers, J., "Flutter Analysis of a Two-Dimensional Airfoil Containing Structural Nonlinearities," National Aeronautical Establishment, Aeronautical Note LR-618; National Research Council (Canada) No. 27833, Ottawa, 1987.

[15] Price, S. J., Alighanbari, H., and Lee, B. H. K., "Post-Instability Behaviour of a Two-Dimensional Airfoil with a Structural Nonlinearity," *Journal of Aircraft*, Vol. 31, No. 6, 1994, pp. 1395–1401.

[16] Price, S. J., Alighanbari, H., and Lee, B. H. K., "The Aeroelastic Response of a Two-Dimensional Airfoil with Bilinear and Cubic Structural Nonlinearities," *Journal of Fluids and Structures*, Vol. 9, No. 2, 1995, pp. 175–193.